



UNIVERSITÀ POLITECNICA DELLE MARCHE  
Repository ISTITUZIONALE

Comparative fragility methods for seismic assessment of masonry buildings located in Muccia (Italy)

This is the peer reviewed version of the following article:

*Original*

Comparative fragility methods for seismic assessment of masonry buildings located in Muccia (Italy) / Chieffo, N.; Clementi, F.; Formisano, A.; Lenci, S.. - In: JOURNAL OF BUILDING ENGINEERING. - ISSN 2352-7102. - STAMPA. - 25:(2019), p. 100813. [10.1016/j.jobe.2019.100813]

*Availability:*

This version is available at: 11566/267525 since: 2022-05-25T11:17:31Z

*Publisher:*

*Published*

DOI:10.1016/j.jobe.2019.100813

*Terms of use:*

The terms and conditions for the reuse of this version of the manuscript are specified in the publishing policy. The use of copyrighted works requires the consent of the rights' holder (author or publisher). Works made available under a Creative Commons license or a Publisher's custom-made license can be used according to the terms and conditions contained therein. See editor's website for further information and terms and conditions.

This item was downloaded from IRIS Università Politecnica delle Marche (<https://iris.univpm.it>). When citing, please refer to the published version.

note finali coverage

(Article begins on next page)

# Comparative fragility methods for seismic assessment of masonry buildings located in Muccia (Italy)

Nicola Chieffo<sup>1</sup>, Francesco Clementi<sup>2</sup>, Antonio Formisano<sup>3</sup>, Stefano Lenci<sup>4</sup>

<sup>1</sup>Department of Civil Engineering, Politehnica University of Timișoara, Romania

<sup>2,4</sup> Department of Civil Engineering, Construction and Architecture,  
Polytechnic University of Marche

<sup>3</sup>Department of Structures for Engineering and Architecture, University of Naples “Federico II”

<sup>1</sup>nicola.chieffo@student.upt.ro, <sup>2</sup>francesco.clementi@univpm.it, <sup>3</sup>antoform@unina.it, <sup>4</sup>lenci@univpm.it

## Abstract

The current paper focuses on a sector of the historic centre of Muccia, in the district of Macerata (Italy), affected by the seismic sequence that involved Central Italy in 2016. *The main goal is the comparison in terms of fragility curves among two vulnerability assessment methodologies, empirical and mechanical ones.* The study area has been structurally and typologically identified according to the Building Typology Matrix (BTM). The physical vulnerability analysis of the urban-sector was performed through the application of a specific form for masonry building aggregates. Consecutively, an isolated masonry building, damaged after the seismic sequences, has been selected as a case study. On the assessed building, empirical fragility curves are presented according to the Guagenti & Petrini's correlation law. Furthermore, the numerical model was built by using the macro-element approach, in order to simulate the seismic behaviour of the analysed structure. Mechanical properties of masonry were defined according to the New Technical Codes for Constructions (NTC18), assuming a limited knowledge level (LCI). A refined mechanical fragility functions have been derived and compared to the empirical ones.

From the results achieved, the empirical method tends to overestimate by 5% and 10% the expected damage for slight and moderate thresholds. Contrary, for PGA values greater than 0,3g the damage levels decreased by 30% and 20%, with reference to the near collapse and collapse conditions, respectively.

**Keywords:** Masonry buildings, empirical method, mechanical method, vulnerability assessment, damage scenarios, fragility curves.

60  
61  
62 **1. State of Art**  
63

64 The seismic risk assessment is a multivariate problem based on the estimation of three major factors  
65 such as vulnerability (V), hazard (H) and exposure (E). The combination of these factors allows to  
66 qualitatively and quantitatively describe the risk in a given area and allows estimates of possible  
67 losses as a result of catastrophic events. The estimation of these three factors is very important for the  
68 planning of interventions (on an urban scale) of risk mitigation [1, 2]. The concept of vulnerability,  
69 V, is mainly based on the capacity of a building to suffer specific damage due to a seismic event. The  
70 exposure, is connected to the nature, quantity and value of the properties and activities of the area  
71 that can be influenced directly or indirectly by a seismic event and finally, the hazard is understood  
72 as the probability of occurrence of the asymptomatic event of a certain intensity in a specific site, and  
73 depends mainly on the geographic position and the geological characteristics of the site in which the  
74 event is expected. The seismic hazard represented by the frequency and the force of the earthquakes  
75 that affect it, or by its seismicity. It is defined as the probability that in an area and in a certain time  
76 interval an earthquake occurs that exceeds a threshold of intensity, magnitude or peak acceleration  
77 (PGA).  
78

79 Masonry has been one of the most popular construction materials developed during the centuries as  
80 it provided economic and functional solutions worldwide. Nevertheless, the existing unreinforced  
81 masonry buildings (URM) are typically identified as "*potential risk factors*" due to the behaviour of  
82 masonry that is very complicated to be predicted. In fact, when the URM buildings are subjected to  
83 shaking due to the earthquake, the mass of the walls and lightweight flexible diaphragms, leads to a  
84 rigid-fragile global behavior that triggers the possible collapse mechanisms increasing the possibility  
85 of repercussions on society (physical and economic losses). Generally, these constructions have been  
86 designed to resist only gravity loads, offering a very low resistance to seismic actions [3, 4].  
87

88 The URM response depends on several aspects that mainly affect the ductility piers and strength of  
89 the walls [5]. The failure mode is affected by several parameters, such as the vertical compression  
90 due to gravity loads, the wall aspect ratio, the boundary conditions, and the relative strength between  
91 mortar joints and units. In the past, strong earthquakes have caused considerable damage given the  
92 poor consistency of the building samples. The damage is attributed to an inadequate structural  
93 integrity and to the lack of connection between the orthogonal walls which results in typical shear  
94 cracking and disintegration of the walls with consequent partial or total collapses [6, 7]. It seems  
95 evident that the many uncertainties, mainly associated with the mechanical characteristics of the basic  
96 material (not homogeneous and anisotropic) and construction techniques, negatively influence the  
97 structures' capacity to overcome a seismic event [8].  
98  
99  
100  
101  
102  
103  
104  
105  
106  
107  
108  
109  
110  
111  
112  
113  
114  
115  
116  
117  
118

119  
120  
121 Focusing on historical centers, they are characterized by numerous buildings of immeasurable  
122 architectural and cultural value. In fact, the large number of old masonry buildings in many of the  
123 Italian seismic areas represents one of the crucial points for the preservation and protection of the  
124 existing heritage.  
125  
126

127  
128 The heterogeneity of buildings formed in aggregate is a very delicate aspect as it requires a significant  
129 level of knowledge on every single building that is however very small compared to numerical  
130 analysis methodologies. Nevertheless, ordinary buildings located in the historical centres are often  
131 made of different quality masonries and constructive details that can highlight deficiencies with  
132 respect to safety conditions against seismic actions [9, 10]. A significant number of proposals based  
133 on simplified modeling approaches is already available in the scientific literature. Most of them are  
134 based on the assumption that the masonry wall is represented as a set of one-dimensional macro-  
135 elements (piers and spandrels), connected by nodes in such a way as to reproduce the behavior of the  
136 wall by an equivalent frame, which gives the possibility of using conventional numerical methods of  
137 structural mechanics [11, 12]. Other advanced methods, proposed in [13, 14], investigates the seismic  
138 response by means of non-linear dynamic analysis assuming that masonry behaves as a damaging-  
139 plastic material with almost vanishing tensile strength. Generally, the presence of vulnerability factors  
140 is a fundamental feature that significantly decreases the strength of the walls, influencing the damage  
141 distribution mainly due to out-of-plane actions. Furthermore, it has been stated that a preliminary  
142 structural assessment through kinematic limit analysis on partial failure mechanisms may be reliable  
143 only after a proper estimation of the different structural elements playing a role in the horizontal  
144 behavior (e.g. interlocking between walls, typology of masonry, distribution of horizontal loads,  
145 constraints and dead loads distribution, etc.). The comparison between the numerical results and the  
146 damage survey showed that the numerical approach used in [15] may be an adequate tool to properly  
147 evaluate the seismic response of historical masonry buildings. However, it would be unreasonable to  
148 perform numerical analyses on each individual building within historic centers.  
149  
150

151  
152 To this purpose, the large-scale evaluation methodologies are mainly based on observational data for  
153 a significant sample of buildings, therefore, for the evaluation of the seismic vulnerability of the  
154 aggregates, rapid methods are generally used (vulnerability index method) for an appropriate  
155 vulnerability estimate and the attribution of the vulnerability class is supported on information on  
156 buildings (drawings and on-site inspections) [13, 14]. The peculiarity of this methodology lies in the  
157 fact that it can be combined with the macroseismic method for the assessment of damage scenarios.  
158  
159 The macroseismic methodology, therefore, foresees to be able to evaluate the susceptibility of a stock  
160 of buildings to the variation of the hazard which in the specific case is defined as macroseismic  
161  
162  
163  
164  
165  
166  
167  
168  
169  
170  
171  
172  
173  
174  
175  
176  
177

178  
179  
180 intensity EMS-98 [15]. The possibility of identifying the most vulnerable sample of buildings, allows  
181  
182 previously to mitigate the effects of the seismic phenomenon [16].

183 Based on these premises, the main target of this research work is to identify the seismic response of  
184  
185 the isolated building by means of fragility curves developed using different approaches in order to  
186  
187 obtain a synthetic damage parameter under different grade earthquakes.  
188

## 189 190 191 192 193 194 195 196 197 198 **2. Historical background of the City of Muccia**

199  
200 The City of Muccia (Fig.1) is an Italian town of 911 inhabitants in the province of Macerata in the  
201  
202 Marche region. The Municipality is 454 m on the sea level with an area of 25.91 Km<sup>2</sup>. On the banks  
203  
204 of the Chienti River, located at an important road junction since antiquity, Muccia hosts numerous  
205  
206 archeological finds, remarkable 15<sup>th</sup> century churches and a wonderful Franciscan hermitage, oasis  
207  
208 of peace and meditation. Since prehistory, has been characterised as a knot of important  
209  
210 communication channels. In the middle Ages, under the name of Mutia, it was a strategic place for  
211  
212 the processing and trade of grains, so that the lordship of Da Varano di Camerino erected a castle in  
213  
214 defense of mills [17].  
215  
216  
217  
218  
219  
220  
221  
222  
223  
224  
225  
226  
227  
228  
229  
230  
231  
232  
233  
234  
235  
236

237  
238  
239  
240  
241  
242  
243  
244  
245  
246  
247  
248  
249  
250  
251  
252  
253  
254  
255  
256  
257  
258  
259  
260  
261  
262  
263  
264  
265  
266  
267  
268  
269  
270  
271  
272  
273  
274  
275  
276  
277  
278  
279  
280  
281  
282  
283  
284  
285  
286  
287  
288  
289  
290  
291  
292  
293  
294  
295



Figure 1. The city of Muccia in the Marche region of Italy.

On January 1436 it was sacked by the troops of Francesco Sforza when he occupied the Marche. His proximity to Camerino makes him presumptuous. Next, with the Napoleonic Kingdom of Italy, was part of the department of Tronto, district of Camerino, canton of the same name. With the district of Camerino, he passed to the Musone department in 1811. The definitive destruction of the Musone took into account decree no. 118 of July 14<sup>th</sup> 1807, and brought together in a single municipality several nearby locations, so that none of them had a population of less than 1000 inhabitants. During the Restoration, it was common under the governorate of Camerino, in the homonymous delegation. The advent of the Unity of Italy, the commune became part of the province of Macerata in Camerino's mandate. Muccia is also a center characterized by numerous archeological finds and sites of interest, among which are the Church of Santa Maria di Varano, with an octagonal plan, the "Tower of Massa", "Torraccia" at Mentori.s.l.m. 808 at Massaprofoglio (Fig. 2).



(a)



(b)

Figure 2. Archeological site: a) Sant Maria di Varano Church; b) Massaproglio Castle.

## 2.1. The Central Italy seismic sequences

The first main-shock occurred August 24<sup>th</sup>, 2016 had its epicenter in the province of Rieti (near the municipality of Accumoli), but it also affected the provinces of Perugia, Ascoli Piceno, L'Aquila and Teramo. The municipalities closest to the epicenter are: Accumoli, Amatrice, Arquata del Tronto. The maximum moment magnitude recorded,  $M_w$ , was equal to 6,0. The area affected by the aftershocks, which in a first approximation represents the extension of the activated fault, is approximately 25 km and is aligned in the sense NNO - SSE. Subsequently, several aftershocks have been recorded, the largest of which are in the area of Norcia (PG) with magnitude equal to 5,4. The hypocenter depths of the replicas are modest, almost all within the first 10 km [18].

Two powerful replicas took place on October 26<sup>th</sup>, 2016 with epicentres at the Umbria-Marche border between the municipalities of Visso, Ussita and Castelsantangelo sul Nera with a magnitude of 5,9. On October 30<sup>th</sup>, 2016, the strongest shock, magnitude 6,5, with the epicenter between the municipalities of Norcia and Preci, in the Province of Perugia was recorded. The observations and preliminary analyses prepared by INGV [19] through seismological surveys, allowed a first interpretation of the event (Figure 3).

355  
 356  
 357  
 358  
 359  
 360  
 361  
 362  
 363  
 364  
 365  
 366  
 367  
 368  
 369  
 370  
 371  
 372  
 373  
 374  
 375  
 376  
 377  
 378  
 379  
 380  
 381  
 382  
 383  
 384  
 385  
 386  
 387  
 388  
 389  
 390  
 391  
 392  
 393  
 394  
 395  
 396  
 397  
 398  
 399  
 400  
 401  
 402  
 403  
 404  
 405  
 406  
 407  
 408  
 409  
 410  
 411  
 412  
 413

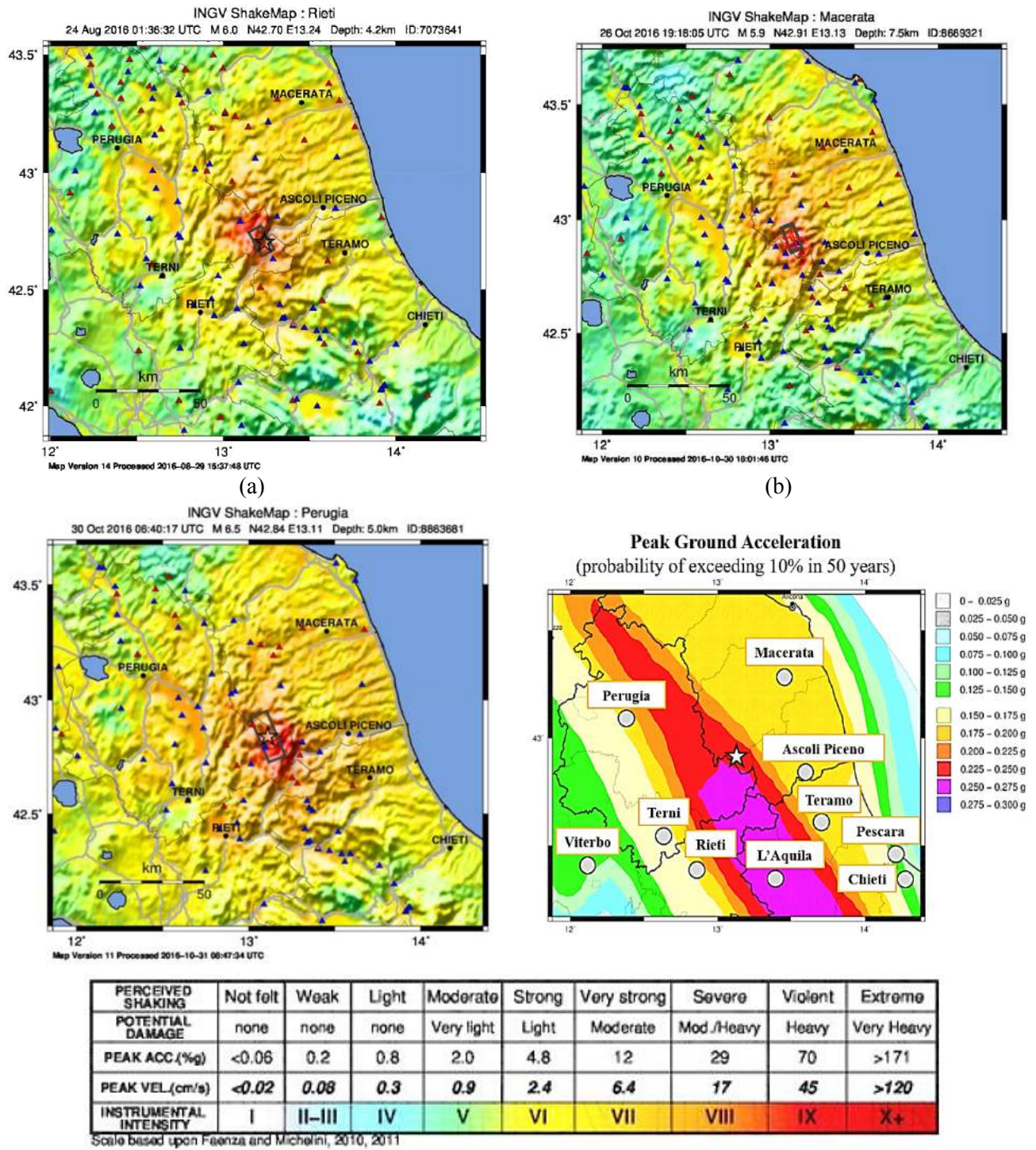


Figure 3. Shake maps of the events occurred: (a) August 24<sup>th</sup>, 2016; (b) October 26<sup>th</sup>, 2016 and (c) October 30<sup>th</sup>, 2016 [19].

The seismogenetic area was characterized by the presence of different segments of fault with high structural complexity. The focal mechanisms (*slip*) allow identifying the type of movement that occurred following a specific earthquake, then how the area moved in response to tectonic deformation as reported in Fig. 4.



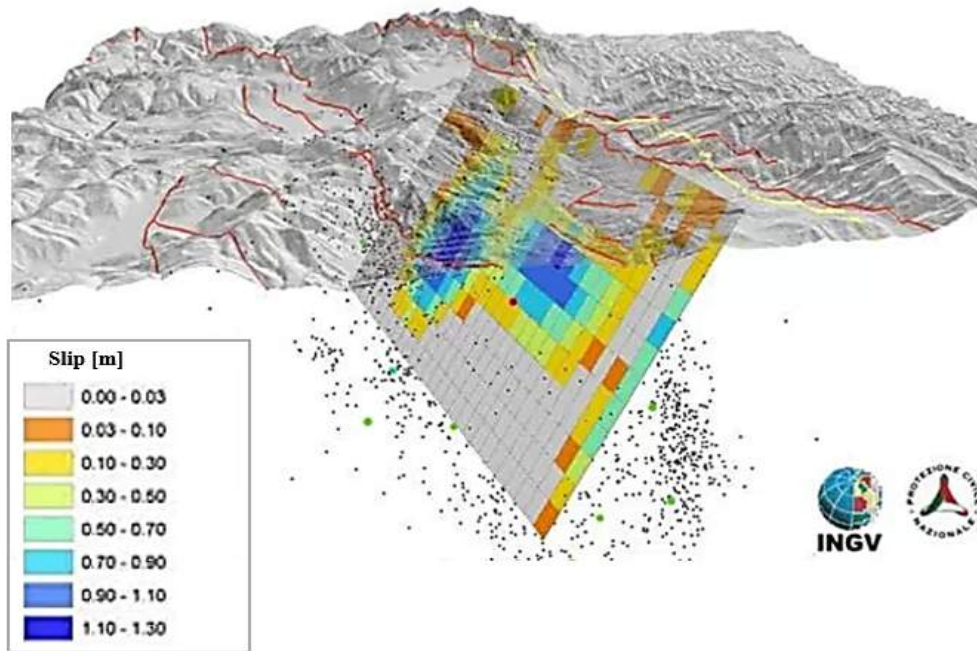


Figure 4. The focal mechanism occurred [19].

Already from the morning of August 24<sup>th</sup>, following the first excavations in the area, some surface fractures (cosmic effects) have been discovered and mapped [20], showing a continuity of at least 1,8 km from the Monte Vettore side. The maximum of cosismic deformation seems to be found near Accumoli (Fig. 5).

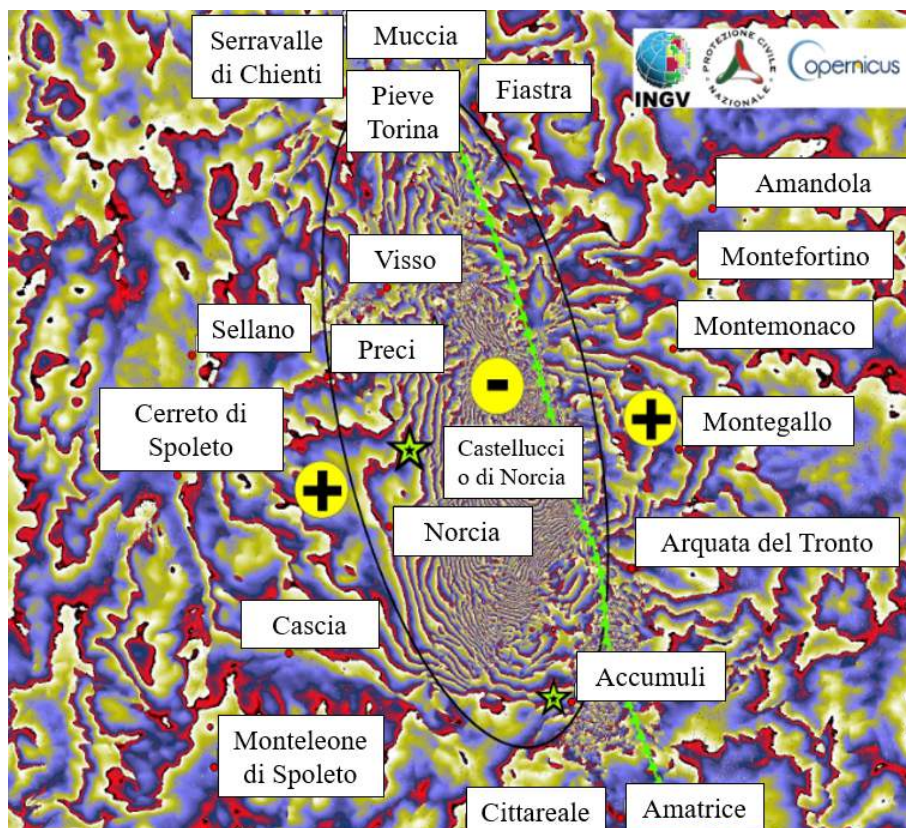


Figure 5. The coseismic deformation map [20].

473  
474  
475 The area was characterised by a vertical extension indicated with "+" in the previously figure, while,  
476 the zone subject to a depression, is indicated with the symbol "-". The green line indicates the seismic  
477 fault that generated the earthquake.  
478  
479  
480

### 481 3. Seismic vulnerability assessment of the historical centre of Muccia

#### 482 3.1. Characterisation of the study area

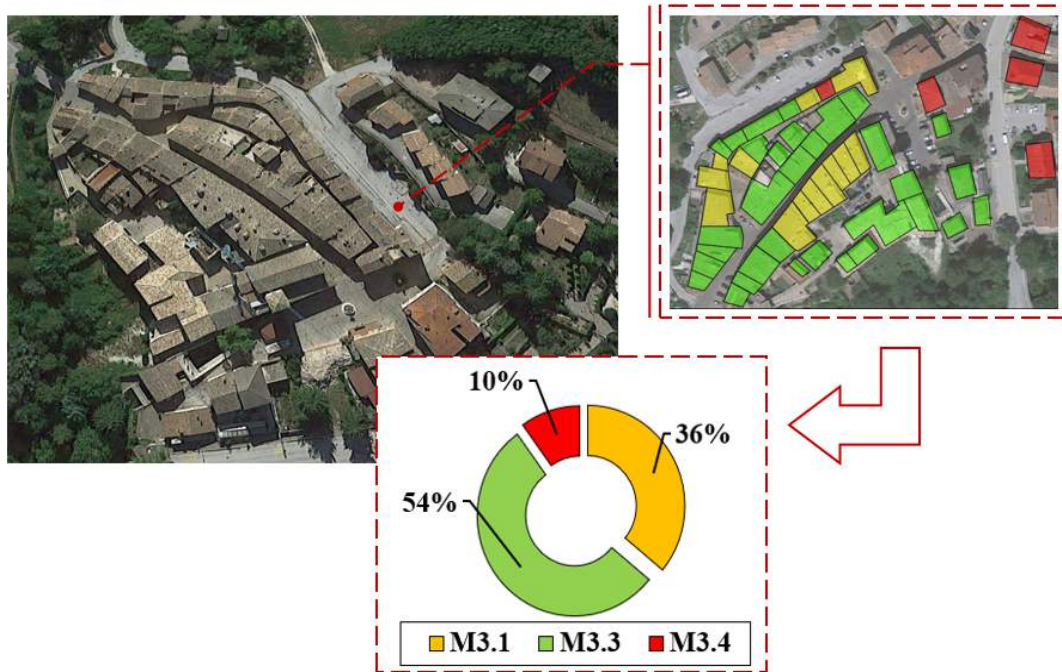
483  
484  
485 The sub-urban sector analysed (Fig.6) is to be considered homogeneous from a typological and  
486 structural point of view. It consists of 50 masonry buildings dating back to the 19<sup>th</sup> century.  
487  
488  
489



509 Figure 6. The sub-urban sector identification.

510  
511  
512 According to Building Typology Matrix (BTM) [21], this sector is composed by 50 buildings:  
513 M3.1 class masonry structures with steel floors (36% of the cases) and M3.3 class masonry  
514 structures with wooden floors (54%) and M3.4 masonry structures with rc floors (10%) (Fig.7).  
515  
516  
517  
518  
519  
520  
521  
522  
523  
524  
525  
526  
527  
528  
529  
530  
531

532  
533  
534 Typological Characterisation  
535



556 Figure 7. Typological characterisation of sub-urban sector.

557  
558 The masonry aggregates under study generally develop in elevation from 2 to 3 stories. The inter-  
559 storey height is about 3.00-4.00 m for the first level and 3.00-3.50 m for other floors.

560  
561 Roofing structures are often composed of double pitch r.c. beams with clay tile covering or wooden  
562 elements. In many cases the presence in the walls of an incongruous and brittle binder, which lost over  
563 time its characteristics, compromises the static nature of the buildings themselves and, sometimes, of  
564 the whole aggregate. The presence of these vulnerability factors increases the possibility of collapse  
565 and instability of the historical built-up when subjected to an impacting seismic action (Fig. 8).  
566  
567  
568



583 Figure 8. Building conformation: a) vertical configuration; b) structural heterogeneities.  
584  
585  
586  
587  
588  
589  
590

### 3.2. Seismic vulnerability assessment

Aiming at implementing a quick seismic evaluation procedure for masonry aggregates, it has been used the new vulnerability form proposed in Table 1 [22], which has been used in recent years for the seismic vulnerability assessment of several historical masonry aggregate [23, 24] (Table. 1).

Table 1. The vulnerability form for buildings in aggregate.

Parameters	Class Score, $S_i$				Weight, $W_i$
	A	B	C	D	
<b>1. Organization of vertical structures</b>	0	5	20	45	1,00
<b>2. Nature of vertical structures</b>	0	5	25	45	0,25
<b>3. Location of the building and type of foundation</b>	0	5	25	45	0,75
<b>4. Distribution of plan resisting elements</b>	0	5	25	45	1,50
<b>5. In-plane regularity</b>	0	5	25	45	0,50
<b>6. Vertical regularity</b>	0	5	25	45	0,50
<b>7. Type of floor</b>	0	5	15	45	0,80
<b>8. Roofing</b>	0	15	25	45	0,75
<b>9. Details</b>	0	0	25	45	0,25
<b>10. Physical conditions</b>	0	5	25	45	1,00
<b>11. Presence of adjacent building with different height</b>	-20	0	15	45	1,00
<b>12. Position of the building in the aggregate</b>	-45	-25	-15	0	1,50
<b>13. Number of staggered floors</b>	0	15	25	45	0,50
<b>14. Structural or typological heterogeneity among adjacent S.U.</b>	-15	-10	0	45	1,20
<b>15. Percentage difference of opening areas among adjacent facades</b>	-20	0	25	45	1,00

This new form is based on the method of the vulnerability index devised by Benedetti and Petrini [25]. This survey form is composed of 10 basic parameters and has been widely used in the past to survey the main structural system and the fundamental seismic deficiencies of isolated buildings in the case of an earthquake. In order to consider the structural interaction between adjacent buildings, not considered in the previously mentioned method, a new form has been adopted. The new form of investigation, appropriately conceived for the aggregates of masonry buildings, is conceived by adding five new parameters to the ten basic parameters of the original form. These new parameters take into account the interaction effects between the aggregate structural units under earthquake [26].

Formally, the methodology is based on the evaluation of a vulnerability index,  $I_v$ , for each S.U. of the aggregate intended as the weighted sum of the 15 parameters mentioned above. In Table 1, it is possible to notice how these parameters are distributed into four classes (A, B, C and D) with scores,  $S_i$ , of growing vulnerability.

A weight,  $W_i$ , is associated to each parameter that can range from 0,25 for the less important parameters to a maximum of 1,50 for the most important ones. According to this, the vulnerability index,  $I_v$ , can be calculated according to the following equation:

$$I_V = \sum_{i=1}^{15} S_i \times W_i \quad (1)$$

Subsequently,  $I_v$  is normalised in the range  $[0 \div 1]$ , adopting the notation  $V_I$ , by means of the following relationship:

$$V_I = \left[ \frac{I_V - (\sum_{i=1}^{15} S_{\min} \times W_i)}{\sum_{i=1}^{15} [(S_{\max} \times W_i) - (S_{\min} \times W_i)]} \right] \quad (2)$$

Based on these premises, the statistical distributions of the global vulnerability of the sub-urban sector analysed has been depicted in Figure 9.

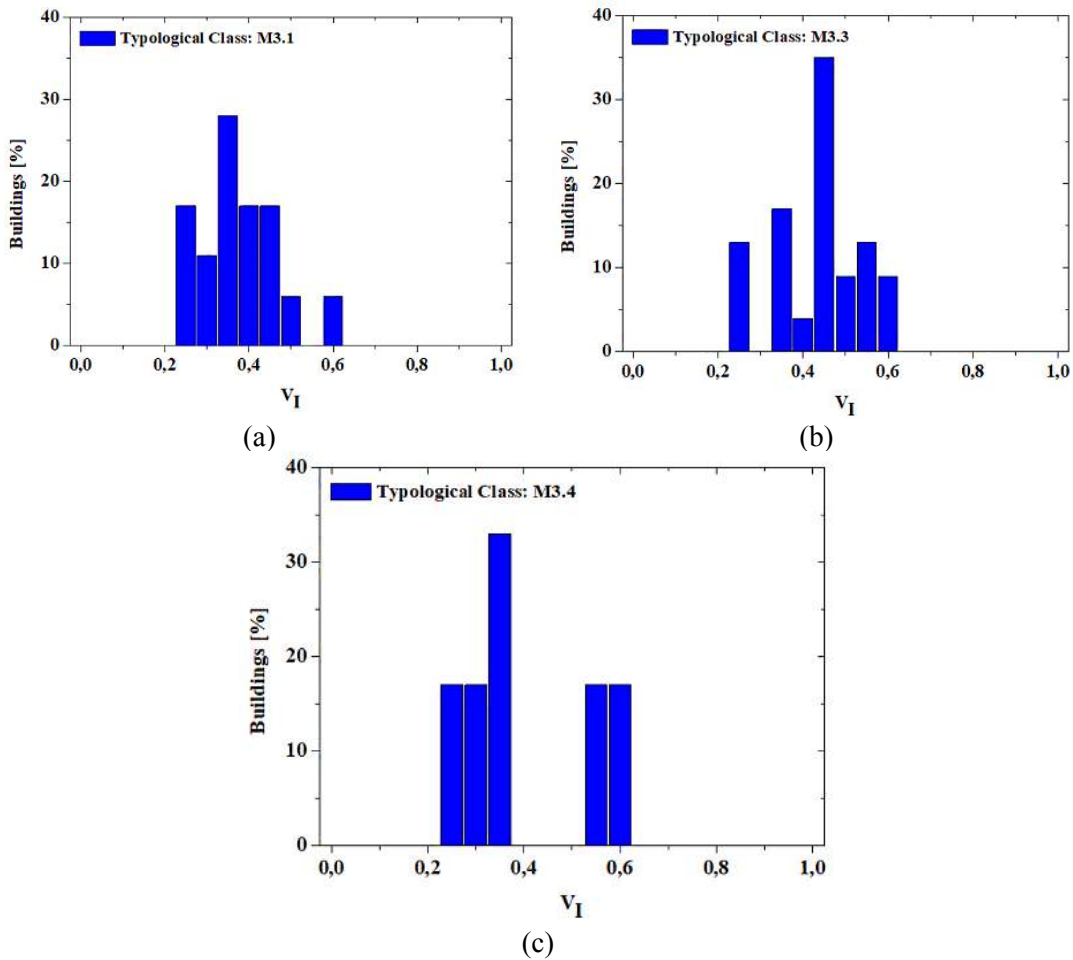


Figure 9: Vulnerability frequency distributions of the sample of buildings belonging to (a) M3.1, (b) M3.3 and (c) M3.4 typological classes.

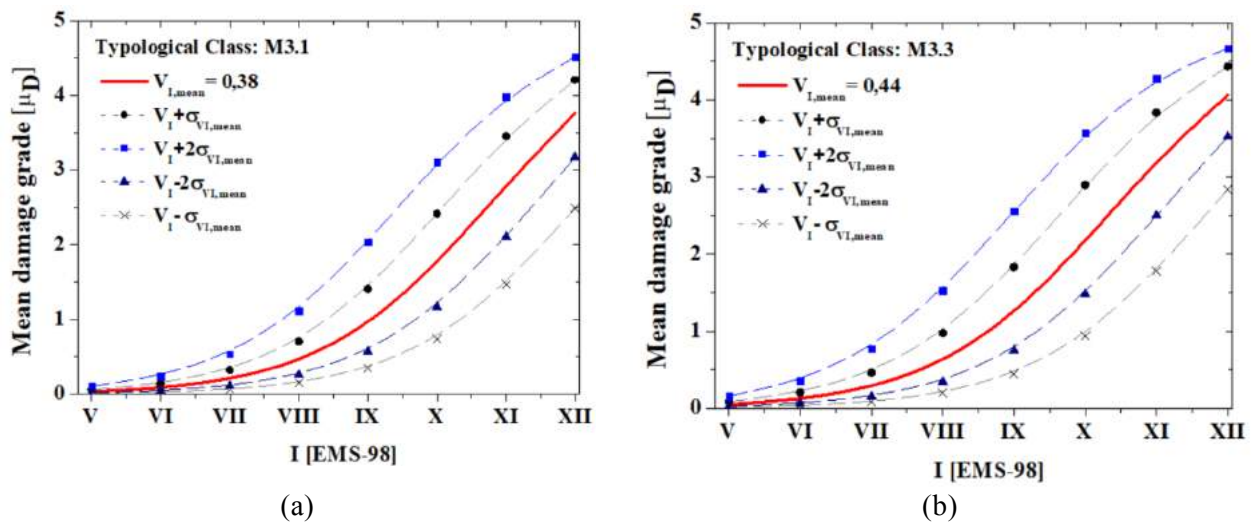
From the analysis of the results, it is worth noting how 28% of buildings belonging to the typological class M3.1 have a vulnerability index of 0,42 and only 5% have an index of 0,50 and 0,60. Similarly, for the class M3.3, 34% of the sample will have a vulnerability index of 0,42 and has a minimum of 3% associated with a vulnerability index of 0.38. Considering the M3.4 class, 35% of the buildings case have index of 0,38 and the 15% have index equal to 0,20 and 0,60, respectively.

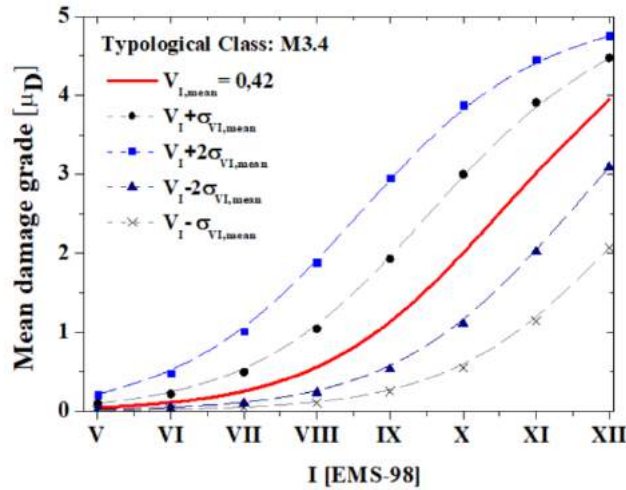
### 3.3. Typological vulnerability curves

The proposed procedure, developed by [27], allows correlated macroseismic intensity, according to the EMS-98 scale, with the expected mean damage grade mathematically expressed by Eq. (3).

$$\mu_D = 2,5 \left[ 1 + \tanh \left( \frac{I + 6,25 \times V_I - 13,1}{Q} \right) \right] \quad (3)$$

As can be seen, the vulnerability curves depend on three variables: the vulnerability index ( $V_I$ ), the hazard, expressed in terms of macroseismic intensity ( $I$ ), and a ductility factor  $Q$ , ranging from 1 to 4, which describes the ductility of typological classes of buildings and has been assumed as equal to 2,3 as proposed by [9]. The method refers to the vulnerability model implicitly included in the EMS-98 and accounts for the uncertainty in the attribution of the different building typologies to the EMS-98 vulnerability classes and for the variability in the building-to building vulnerability within the same typology. Therefore, the mean vulnerability curves shown in Figure 10 have been plotted in order to estimate the collapse probability of analysed buildings for different scenarios ( $V_I - \sigma_{V_I, Mean}$ ;  $V_I + \sigma_{V_I, Mean}$ ;  $V_I + 2\sigma_{V_I, Mean}$ ;  $V_I + 2\sigma_{V_I, Mean}$ ) [28, 29].





(c)  
Figure 10: Mean typological vulnerability curves for the sample of buildings examined.

## 4 Estimated damage scenario

### 4.1 Damage model prediction

Scenario analysis allows to analyse in detail the damage associated with a generic structural system when subjected to a natural event. Referring to the case study examined, the damage associated with a seismic event is considered. In particular, according to the Section 2.1, a set of magnitudes, enclosed in the range [5,4 - 6,5] have been selected.

The severity of the damage was analysed thanks to predictive analysis in which, during the earthquake, buildings with the same structural characteristics would be subject to a damage that decreases when increase the epicentral distance. Subsequently, the attenuation law defines the macroseismic intensity according to EMS-98 by the formula proposed by Crespellani, [30] and reported in Equation (4).

$$I_{EMS-98} = 6,39 + 1,756M_w - 2,747 \times \ln(R + 7) \quad (4)$$

where,  $M_w$  is the moment magnitude occurred and  $R$  is the site-source distance expressed in Km. According to the scale EMS-98, six damage levels,  $D_k$ , each one associated to a damage score  $k$ , ranging from 0 to 5, are defined:  $D0$ : no damage;  $D1$  (*moderate damage*): with hair-line cracks in very few walls and fall of small pieces of plaster only;  $D2$  (*substantial damage*): structural damage and moderate non-structural damage. Cracks in many walls with fall of fairly large pieces of plaster. Partial collapse of chimneys;  $D3$  (*significant damage*): intensive structural damage and heavy non-structural damage, with large and extensive cracks in most walls; roof tiles detachment; chimneys fracture at the roof line; failure of individual non-structural elements (partitions, gable walls); activation of the first out-of-plane mechanisms;

827  
828  
829  
830  
831  
832  
833  
834  
835  
836  
837  
838  
839  
840  
841  
842  
843  
844  
845  
846  
847  
848  
849  
850  
851  
852  
853  
854  
855  
856  
857  
858  
859  
860  
861  
862  
863  
864  
865  
866  
867  
868  
869  
870  
871  
872  
873  
874  
875  
876  
877  
878  
879  
880  
881  
882  
883  
884  
885

*D4 (partial collapse)*: extended damage and very heavy non-structural damage, with serious wall failures; partial structural failure of roofs and floors; *D5 (collapse)*: collapse to both non-structural and structural parts, with total or near total collapse of the whole building. Considering the representative damage parameter  $\mu_D$ , the expected number of buildings that undergo a certain damage level has been determined (Fig. 11).

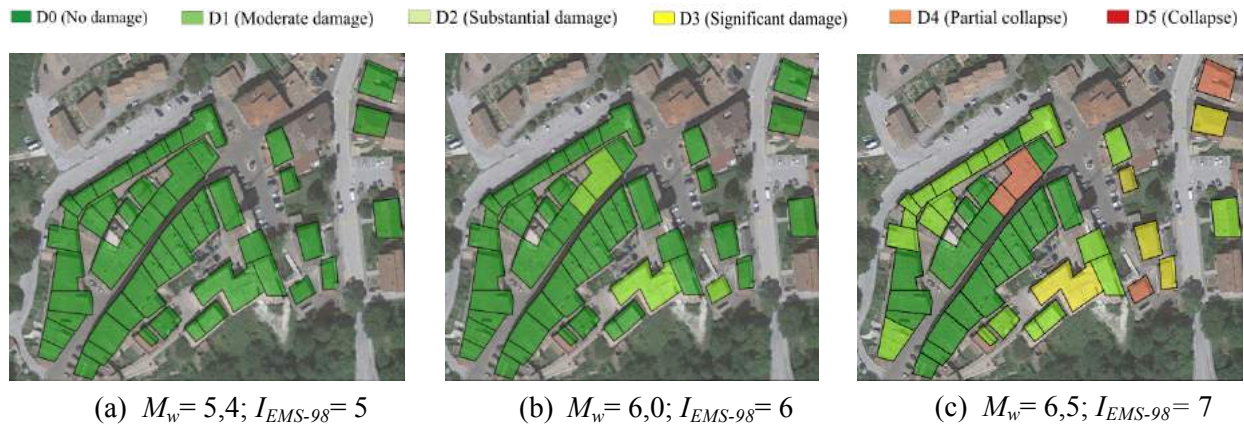


Figure 11. Damage scenarios for a set of moment magnitudes occurred.

A complete damage distribution has been defined from the scenario previously achieved. The conditional probability,  $P[D_k > D_i | M_w; R]$ , of exceeding a certain damage state,  $D_k$ , varying the magnitude,  $M_w$ , and epicentral distances,  $R$  were presented in Fig. 12.

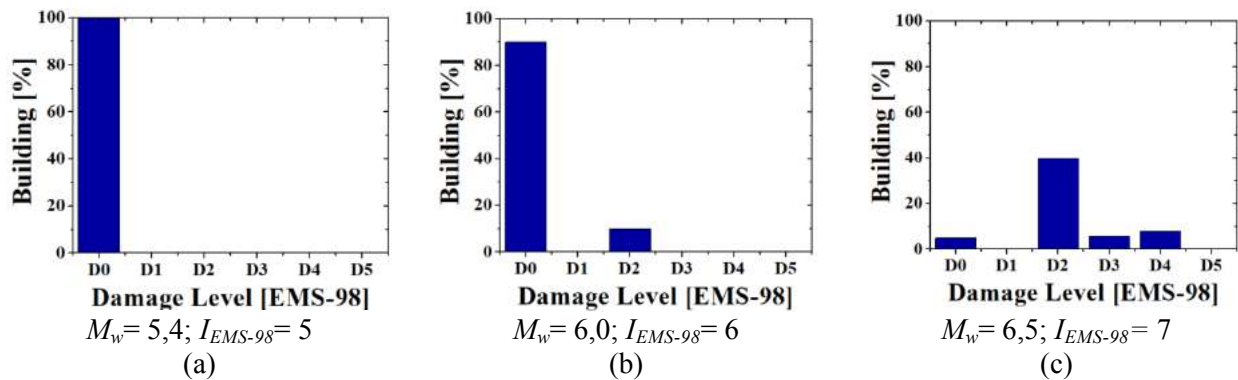


Figure 12. Vulnerability frequency distributions: (a) M3.1, (b) M3.3 and (c) M3.4 typological classes.

As can be seen, for a moment magnitude,  $M_w$ , equal to 5,4, a 100% of building stocks reached damage D0 (No Damage). Consequently, for a magnitude 6,0, the damage distribution shows that a 90% of the cases reached damage D0, instead only 10% of the sample are characterized by damage D2. Furthermore, referring to the event occurred on October 30<sup>th</sup> (epicenter at Accumuli), for a moment magnitude equal to 6,5, the damage distribution provided 40% of the buildings case suffered a D2 damage, 6% suffered a damage D3 and only the 8% of the buildings sample have D4 damage (Extended damage).



886  
887  
888 Moreover, considering the event occurred on October 30<sup>th</sup>, the correlation between the empirical  
889 damage scenario and site-inspection recognition have been showed in Fig.13.  
890  
891



918 Figure 13: Correlation between examined damage scenario and site-inspection.  
919  
920

## 921 4.2 Empirical fragility curves

922  
923 Once the global vulnerability of the entire sub-sector under investigation was defined, it was possible  
924 to focus attention on the case study building indicated with the number 45 in the previous Section 3.  
925 The examined building is in an isolated position (Fig. 14). It is characterized by load-bearing masonry  
926 walls, with wooden floors and pitched roofs with an average height of 3.50 m.  
927  
928

929  
930 The physical conditions denote a widespread damage characterized by the presence of cracks along  
931 the West and North façades, respectively.  
932  
933  
934  
935  
936  
937  
938  
939  
940  
941  
942  
943  
944

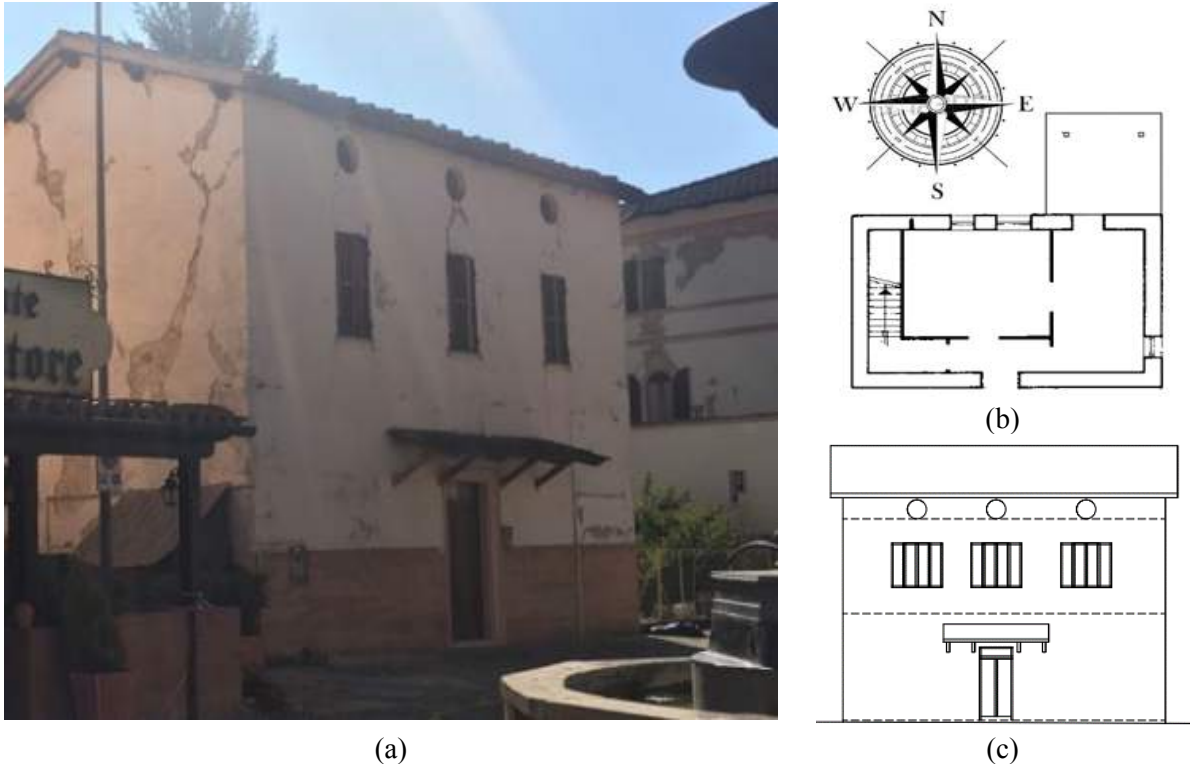


Figure 14: The case study building n.45, (a) street view, intermediate floor (b) and (c) North prospect.

The vulnerability index,  $V_I$ , derived from the index-based method for isolated buildings, is equal to 0,40. Fragility curves are used to define the probability of exceeding a certain degree of damage,  $D_k$  ( $K \in [0 \div 5]$ ). To this purpose, a correlation law proposed by Gaugenti-Petrini [31], is formally used in Equation (5).

$$\ln(PGA) = 0,602I - 7,073 \quad [g] \quad (5)$$

Mathematically, this law provides the variation of PGA as a function of macroseismic intensity,  $I$ , through empirical correlation coefficients  $C_1$  (0,602) and  $C_2$  (7,073). The gotten results are presented in Fig. 15.

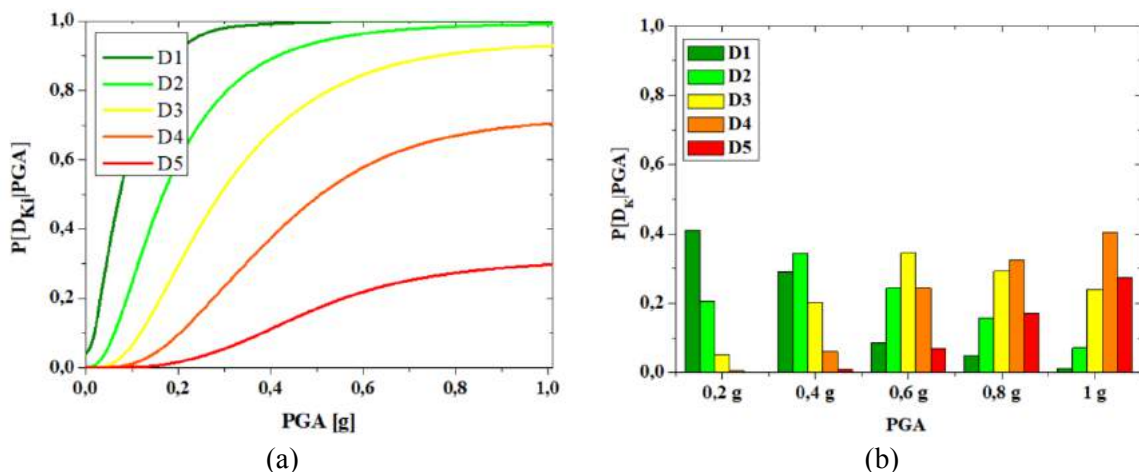


Figure 15: Fragility curves derived by empirical method (a) and damage distribution (b).

## 5 Mechanical vulnerability approach

### 5.1 Assessment of the structural properties

The mechanical characteristics of the materials were chosen according to Italian New Technical Codes for Constructions (NTC18) [32]. The masonry walls, both perimeter and internal, assume a constant thickness in height, without the presence of diffused heterogeneity. The mean compressive strength of masonry ( $f_m$ ) and shear strength ( $\tau_0$ ) are to be considered as minimum values of the range established by NTC18 referring to existing masonry buildings, respectively of 1,00 N/mm<sup>2</sup> and 0,02 N/mm<sup>2</sup>. The modulus of elasticity,  $E$ , have been considered of 870 N/mm<sup>2</sup>, likewise the tangential shear modulus,  $G$ , equal to 290 N/mm<sup>2</sup>. The specific weight of the masonry,  $W$ , is equal to 19,37 KN/m<sup>3</sup> as achieved in Table 2. Moreover, the mechanical properties of the timber elements (oak) are given in Table 3. The expected level of knowledge adopted is LC1 which corresponds to a reduction factor of the mechanical properties of the materials, F.C, equal to 1,35.

Table 2. Mechanical properties of masonry.

<b>Mechanical Properties</b>	<b>Units</b>	<b>Masonry</b>
<b>Modulus of elasticity</b>	$E$ (N/mm <sup>2</sup> )	870
<b>Shear modulus</b>	$G$ (N/mm <sup>2</sup> )	290
<b>Mean compressive strenght</b>	$f_m$ (N/mm <sup>2</sup> )	1,00
<b>Tensile strength</b>	$\tau_0$ (N/mm <sup>2</sup> )	0,02
<b>Specific weight</b>	$W$ (Kg/m <sup>3</sup> )	1937

Table 3. Mechanical properties of wooden elements.

<b>Mechanical Properties</b>	<b>Units</b>	<b>Timber</b>
<b>Modulus of elasticity</b>	$E$ (N/mm <sup>2</sup> )	800
<b>Shear modulus</b>	$G$ (N/mm <sup>2</sup> )	590
<b>Mean compressive strenght</b>	$f_m$ (N/mm <sup>2</sup> )	18
<b>Tensile strength</b>	$\tau_0$ (N/mm <sup>2</sup> )	3,5
<b>Specific weight</b>	$W$ (Kg/m <sup>3</sup> )	570

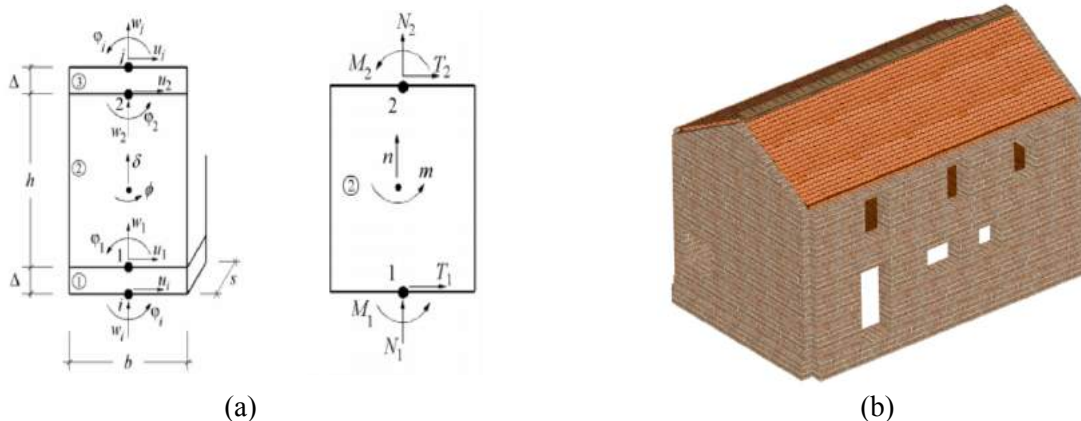
### 5.2 Non-linear static analysis

Non-linear static analysis have been performed by using 3Muri software developed by S.T.A. DATA srl [33]. About numerical modelling, according to the geometrical survey performed, the interstory height is assumed 3.50 m as resorting in the previous section. Wooden floors with thickness of 20 cm have been considered at each level.

Concerning the structural models, the structure is schematized through a series of macroelements interconnected to each other, in some cases leading towards the definition of the so-called "equivalent frames"[34, 35, 36, 37].

1063  
1064  
1065 These macro-elements allow simulating the seismic behaviour of masonry structures, providing  
1066 all the information required for their static linear analyses.  
1067  
1068

1069 The 3Muri software uses macro-elements to generate the threedimensional model of the structure,  
1070 which is then automatically transformed into an assemblage of 3D equivalent frames to perform  
1071 pushover analyses. The typical macro-element used for static linear analyses is schematised with  
1072 the kinematic model reported in Figure 16 (a). The 3D model of the examined housing building,  
1073 where it is apparent that masonry walls are modelled through a mesh of masonry piers and  
1074 spandrels, is depicted in Figure 16 (b).  
1075  
1076  
1077  
1078  
1079



1095  
1096  
1097  
1098  
1099  
1100  
1101  
1102  
1103  
1104  
1105  
1106  
1107  
1108  
1109  
1110  
1111  
1112  
1113  
1114  
1115  
1116  
1117  
1118  
1119  
1120  
1121

Figure 16: The macro-element kinematic model (a) and (b) the 3D building model with macro-elements through the 3Muri software.

The resistance criterias are given on the basis of EN 1998-3 [38] according to which the drift for shear and flexural crack mechanisms are established equal to 0.4% and 0.8% of the ultimate displacement ( $d_u$ ). The shear criteria is based on the diagonal cracks model and adapted to existing masonry buildings in the Italian seismic code, NTC18 [32]. The flexural response is developed by neglecting the tensile strength of the material and assuming a uniformly distributed compression stress distribution at the masonry interface.

Numerical analysis was performed considering a soil category “C” and a design spectrum referred to the Life Safety limit state. Dead and variable loads applied at the different structural levels, as well as partial safety factors for gravity loads combination at the Ultimate Limit State, are shown in Table 4.

Table 4. Design load applied.

Static Load	Intermediate Floor [KN/m <sup>2</sup> ]	Roof [KN/m <sup>2</sup> ]	Partial safety factor
$G_1$	3	3	1,3
$G_2$	2	1	1,3
$Q_k$	2	0,5	1,5

Non-linear static analysis has been performed in the two main directions (X and Y), taking also into account the effect of accidental eccentricities. The analysis results in terms of SDoF capacity curves and corresponding damage are shown in Figure 17.

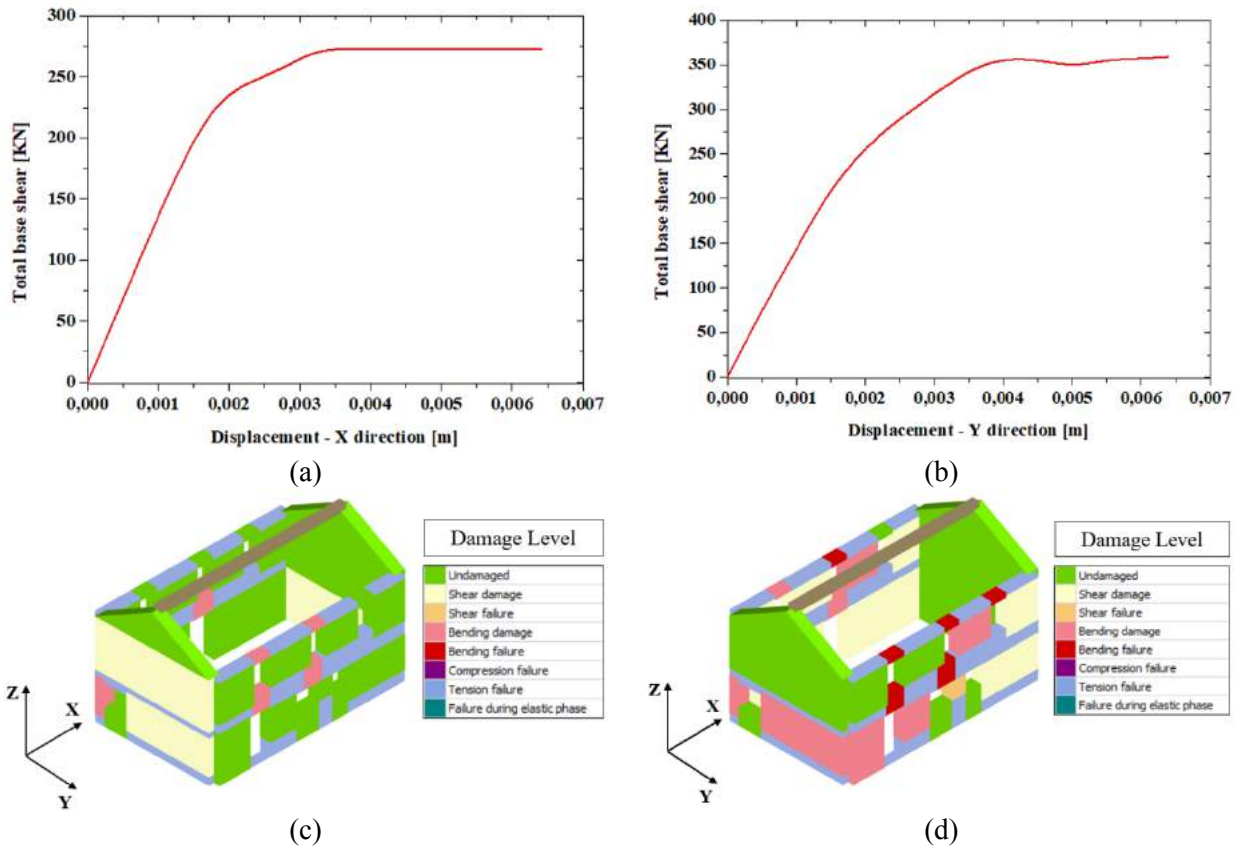


Figure 17: SdoF capacity curves: (a) X direction, (b) Y direction, (c) damage level in X direction and (d) damage level in Y direction.

The capacity curves show that in the X direction the structure has a maximum shear force equal to 272,66 kN with a yield displacement and ultimate displacements,  $D_y^*$  and  $D_u^*$ , equal to 0,0029 m and 0,0064 m, respectively. Similarly, in Y direction, the maximum shear threshold reached is 360,81 kN with the corresponding displacements equal to  $D_y^* = 0,0030$  m and  $D_u^* = 0,0065$  m.

Referring to a failure hierarchy, in X direction the distribution of ductile mechanisms (bending damage) occurs only in some masonry spandrels, whereas the fragile failures, induced by shear, are reached in the East and West façades, respectively. Moreover, the tensile failures are widespread (Figure 17 (c)). Similarly, in Y direction, the damage tends to increase globally. In fact, as can be seen in Figure 17 (d), bending failures occurred in the panel nodes instead the bending damage in some masonry panels. Concerning the shear damage, it is reached in the North and South façades, respectively. In terms of ductility ( $\mu$ ), in X direction the estimated value is 2,87 which corresponds to a percentage increment of 16,7% compared to the ductility calculated in the Y direction equal to 2,4.

The estimated vulnerability indices associated to the two main directions X and Y are evaluated as the ratio between the seismic demand and the corresponding capacity of the building considering the Ultimate Limite State (ULS). In particular, the calculated indexes, in X and Y direction, are 0,38 and 0,48, respectively.

### 5.3 Mechanical fragility curves

Fragility curves express the probability of exceeding a generic damage threshold,  $D_K$ , for a predetermined value of the Intensity Measurement ( $IM$ ), generally represented by the PGA or spectral displacements,  $S_d$ . The evaluation of the fragility curves is carried out according to the methodology proposed by [4]. In particular, four damage thresholds, D1 (slight), D2 (moderate), D3 (near collapse) and D4-D5 (collapse), have been defined and achieved in Table 4. As can be seen, the damage states are intrinsically defined considering the yielding displacement ( $D_y$ ) and ultimate displacement ( $D_u$ ) of the SDoF system.

Table 4. Damage thresholds.

Damage Limit State, $D_i$	Displacement Limit State
$D_1$	Slight $0,7 D_y$
$D_2$	Moderate $D_y$
$D_3$	Near collapse $D_y + 0,5(D_u - D_y)$
$D_4$ - $D_5$	Collapse $D_u$

Methodologically, fragility curves are defined according to Equation (6)

$$P[D_K | PGA] = \Phi \left[ \frac{1}{\beta} \cdot \left( \frac{PGA}{PGA_{D_K}} \right) \right] \quad (6)$$

where,  $\Phi$ , is the cumulative distribution function,  $PGA_{D_K}$  is the median acceleration value associated for each damage threshold and  $\beta$  is the standard deviation of the log-normal distribution.

The dispersion,  $\beta$ , generally depends on the contribution of uncertainties in the seismic demand. This parameter is a function of the ductility,  $\mu$ , of the structural system intended as the ratio between ultimate displacement,  $D_u$ , and the corresponding yielding displacement,  $D_y$ . Based on this assumption, the estimate value of the disperisons are given in Table 5 [39].

Table 5. Standard deviation for each damage thresholds.

Standard Deviation, $\beta_i$	Ductility Limit State
$\beta_1$	Slight $0,25+0,07\ln(\mu)$
$\beta_2$	Moderate $0,2+0,18\ln(\mu)$
$\beta_3$	Near collapse $0,1+0,41\ln(\mu)$
$\beta_4$ - $\beta_5$	Collapse $0,15+0,5\ln(\mu)$

However, in this research work, the fragility functions are derived according to Equation (7)

$$S_{a,e} = \omega^2 \cdot S_{d,e} = \left( \frac{2 \cdot \pi}{T} \right)^2 \cdot S_{D_K} \quad (7)$$

where,  $S_{ae}$  is the expected spectral acceleration,  $T$  is the vibration period of the structural system and  $S_{DK}$  is the spectral displacement associated to the damage thresholds reported in Table 4. Therefore, the fragility curves have been plotted in both directions, longitudinal X and transversal Y, respectively, and depicted in Figure 18.

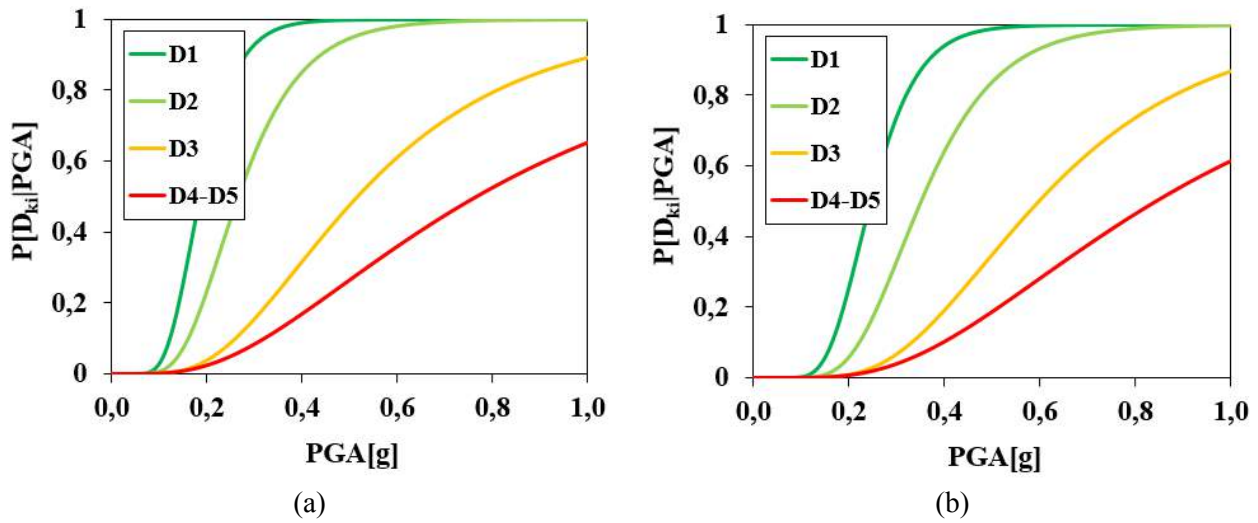


Figure 18: Fragility curves (a) X direction, (b) Y direction, respectively.

As analysed, it is possible to compare the fragility functions for the methods adopted in the present work. The gotten results are depicted in Figure 19.

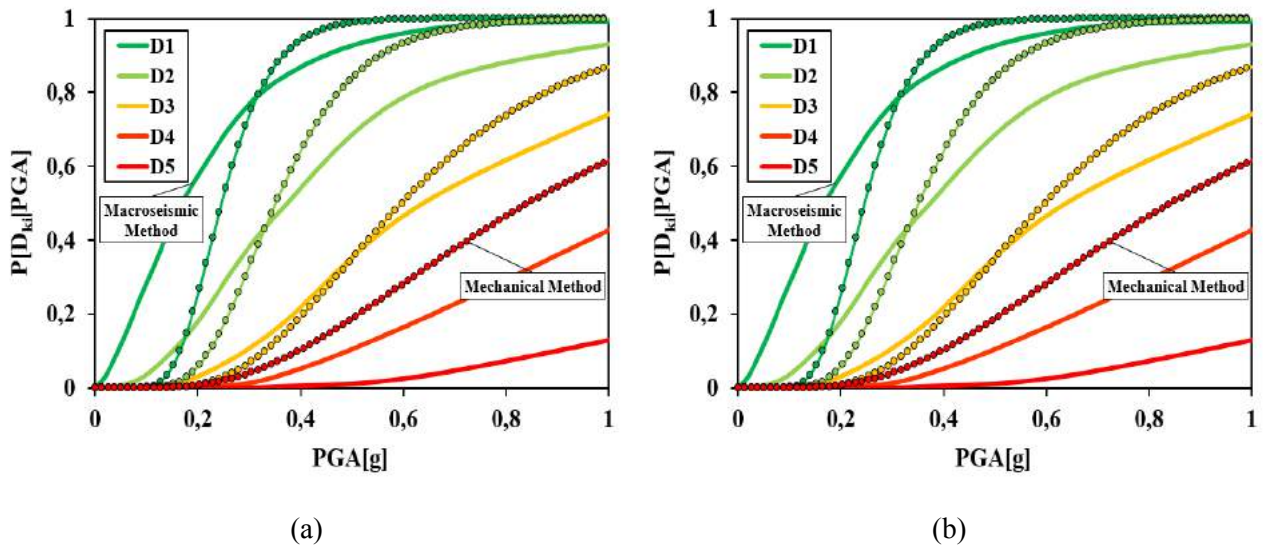


Figure 19: Fragility curves comparison: (a) X direction, (b) Y direction.

1299  
1300  
1301 From the comparison of the applied methodologies, it is possible to notice how the fragility curves  
1302 present different values of the expected damage.  
1303

1304 Generally, this discrepancy is due the different procedures to estimate the damage threshold,  $D_K$ , and  
1305 the uncertainties,  $\beta_i$ .  
1306

1307 On one side, the macroseismic methodology, used for large-scale assessment, adopts an acceleration-  
1308 intensity conversion law for the identification of the PGA range and, subsequently, it allows to plot  
1309 the fragility curves through the cumulative distribution function without taking into account the  
1310 uncertainties,  $\beta$ . On the other hand, the mechanical procedure provides more refined results since it  
1311 takes into account the uncertainties of the structural system and combines them through the lognormal  
1312 distribution.  
1313

1314 Nevertheless, the macroseismic method in both analysis directions, tends to overestimate the damage  
1315 thresholds D1 and D2 by 5% and 10%, respectively, for a spectral acceleration enclosed in the range  
1316  $[0 \div 0,3 \text{ g}]$ . Contrary, for PGA values greater than 0,3g, this method provides an underestimation for  
1317 each damage levels considered. In particular, considering a damage D4 and D5 in both directions, it  
1318 is possible to estimate a mean percentage decrease of 30% and 20%, compared to the mechanical  
1319 procedure. As a conclusion, the mechanical approach can be considered as a very reliable tool in  
1320 predicting fragility curves, since it provides safely more accurate results than the empirical method  
1321 ones.  
1322  
1323  
1324  
1325  
1326  
1327  
1328  
1329

## 1330 **6 Conclusion**

1331  
1332

1333 The study illustrates a comparison between two different approaches for estimating seismic  
1334 vulnerability in terms of expected damage for an isolated masonry building located in the center  
1335 of Muccia. The study area was composed by 50 structural units erected in aggregate, opportunely  
1336 classified according to the BTM in three different classes as M3.1, M3.3, and M3.4, respectively.  
1337 The assessment of seismic vulnerability of the inspected urban-sector has been analysed by means  
1338 of index method approach. The statistical distribution of vulnerability indices shows, globally, a  
1339 medium vulnerability of the stock.  
1340  
1341  
1342  
1343

1344 Afterwards, mean typological vulnerability curves were derived in order to characterize the  
1345 expected global damage varyinig the macroseismic intensity accoding to EMS-98 scale. The  
1346 gotten results shown that, for seismic intensities less than X grade, the expected damage has not  
1347 been relevant, but for high values of seismic intensity ( $X < I_{EMS-98} < XII$ ), the expected damage  
1348 would cause an incipient collapse of the analysed sample.  
1349  
1350  
1351

1352 Analysis of the damage scenario by means parametric approach have been considered using the  
1353 attenuation law in terms of seismic intensity proposed by Crespellani.  
1354  
1355  
1356  
1357



1358  
1359  
1360 Having defined a set of occurred magnitude ( $M_w$ ) and site-source distances ( $R$ ), it has been  
1361 possible to analyse in detail the influence of these factors on an urban scale. The results obtained  
1362 have shown that, the most severe scenario was for  $M_w=6,5$  in which at least 40% of the buildings  
1363 reached damage D2 (Substantial damage) and 8% of the cases reached damage D4 (Extended  
1364 damage).  
1365  
1366

1367  
1368 Subsequently, an isolated building was considered as a case study. The mechanical approach was  
1369 used for the characterisation of the structural model. A 3D model of the examined building, was  
1370 modelled through a mesh of masonry piers and spandrels. The capacity of the structure in  $Y$   
1371 direction showed higher damage than the other orthogonal direction. In fact, considering a failure  
1372 hierarchy a bending and shear damages tend to increase globally. In terms of ductility ( $\mu$ ), the results  
1373 achieved shown an estimated value of  $\mu=2,87$  in  $X$  direction which corresponds to a percentage  
1374 increment of 16,7% compared to the ductility calculated in the  $Y$  direction equal to 2,4. The  
1375 vulnerability indices in  $X$  and  $Y$  directions, evaluated as the ration between the seismic demand and  
1376 the capacity of the structure, were 0,38 and 0,48 respectively.  
1377  
1378

1379  
1380 Consecutively, the fragility curves have been derived for both, empirical and mechanical  
1381 approaches. From the comparison of the applied methodologies, the fragility curves present different  
1382 values of the expected damage. Generally, these differences are due the different procedures to  
1383 estimate the damage threshold,  $D_k$ , and the uncertainties,  $\beta_i$ . In particular, the macroseismic method  
1384 in both analysis directions, tends to overestimate the damage thresholds by 5% and 10%, respectively,  
1385 for a spectral acceleration enclosed in the range  $[0 \div 0,3 \text{ g}]$ .  
1386  
1387

1388  
1389 Contrary, for PGA values greater than 0,3g, this method provides an underestimation for each damage  
1390 levels considered of of 30% and 20%, compared to the mechanical procedure. In conclusion, the  
1391 macroseismic method can be considered an exhaustive approach for urban scale scenario analysis but  
1392 its empirical nature tends to underestimate the damage compared to the mechanical ones. To improve  
1393 the fragility curves, it will therefore be necessary to improve the estimation of the exposure at the  
1394 time of the earthquake and to complete the observational database in order to ensure all the  
1395 information on the surveyed buildings can be processed. For these reasons, the mechanical  
1396 methodology used for estimating the expected damage through fragility curves, is a proven reliability  
1397 method for the evaluation of seismic vulnerability.  
1398  
1399  
1400  
1401  
1402  
1403  
1404  
1405  
1406  
1407  
1408  
1409  
1410  
1411  
1412  
1413  
1414  
1415  
1416

1417  
1418  
1419 **References**  
1420  
1421

- 1422 [1] O.D. Cardona, M.K. van Aalst, J. Birkmann, M. Fordham, G. McGregor, R. Perez, R.S. Pulwarty,  
1423 E.L.F. Schipper, B.T. Sinh, Determinants of Risk : Exposure and Vulnerability Coordinating,  
1424 Managing the Risks of Extreme Events and Disasters to Advance Climate Change Adaptation.  
1425 (2012). doi:10.1017/CBO9781139177245.005.  
1426  
1427
- 1428 [2] A.H. Barbat, M.L. Carreño, L.G. Pujades, N. Lantada, O.D. Cardona, M.C. Marulanda, Seismic  
1429 vulnerability and risk evaluation methods for urban areas. A review with application to a pilot area,  
1430 Structure and Infrastructure Engineering. (2010). doi:10.1080/15732470802663763.  
1431  
1432
- 1433 [3] R. Gonzalez-Drigo, A. Avila-Haro, A.H. Barbat, L.G. Pujades, Y.F. Vargas, S. Lagomarsino, S.  
1434 Cattari, Modernist unreinforced masonry (URM) buildings of barcelona: Seismic vulnerability and  
1435 risk assessment, International Journal of Architectural Heritage. (2015).  
1436 doi:10.1080/15583058.2013.766779.  
1437  
1438
- 1439 [4] P. Lamego, P.B. Lourenço, M.L. Sousa, R. Marques, Seismic vulnerability and risk analysis of the  
1440 old building stock at urban scale: application to a neighbourhood in Lisbon, Bulletin of Earthquake  
1441 Engineering. 15 (2017) 2901–2937. doi:10.1007/s10518-016-0072-8.  
1442  
1443
- 1444 [5] P.B. Lourenço, J.A. Roque, Simplified indexes for the seismic vulnerability of ancient masonry  
1445 buildings, in: Construction and Building Materials, 2006. doi:10.1016/j.conbuildmat.2005.08.027.  
1446  
1447
- 1448 [6] M.P. Ciocci, S. Sharma, P.B. Lourenço, Engineering simulations of a super-complex cultural heritage  
1449 building: Ica Cathedral in Peru, Meccanica. (2018). doi:10.1007/s11012-017-0720-3.  
1450  
1451
- 1452 [7] M. Angelillo, P.B. Lourenço, G. Milani, Masonry behaviour and modelling, in: CISM International  
1453 Centre for Mechanical Sciences, Courses and Lectures, 2014. doi:10.1007/978-3-7091-1774-3\_1.  
1454  
1455
- 1456 [8] **S. Tiberti, G. Milani**, Historic city centers after destructive seismic events, the case of finale Emilia  
1457 during the 2012 Emilia-Romagna earthquake: Advanced numerical modelling on four case studies,  
1458 Open Civil Engineering Journal. (2017). doi:10.2174/1874149501711011059.  
1459  
1460
- 1461 [9] S. Lagomarsino, S. Giovinazzi, Macro seismic and mechanical models for the vulnerability and  
1462 damage assessment of current buildings, Bulletin of Earthquake Engineering. (2006).  
1463 doi:10.1007/s10518-006-9024-z.  
1464  
1465
- 1466 [10] S. Cara, A. Aprile, L. Pelà, P. Roca, Seismic Risk Assessment and Mitigation at Emergency Limit  
1467 Condition of Historical Buildings along Strategic Urban Roadways. Application to the “Antiga  
1468 Esquerra de L’Eixample” Neighborhood of Barcelona, International Journal of Architectural  
1469 Heritage. 12 (2018) 1055–1075. doi:10.1080/15583058.2018.1503376.  
1470  
1471  
1472  
1473  
1474  
1475

1476  
1477  
1478  
1479  
1480  
1481  
1482  
1483  
1484  
1485  
1486  
1487  
1488  
1489  
1490  
1491  
1492  
1493  
1494  
1495  
1496  
1497  
1498  
1499  
1500  
1501  
1502  
1503  
1504  
1505  
1506  
1507  
1508  
1509  
1510  
1511  
1512  
1513  
1514  
1515  
1516  
1517  
1518  
1519  
1520  
1521  
1522  
1523  
1524  
1525  
1526  
1527  
1528  
1529  
1530  
1531  
1532  
1533  
1534

- [11] F. Clementi, E. Quagliarini, F. Monni, E. Giordano, S. Lenci, Cultural Heritage and Earthquake: The Case Study of in Ascoli Piceno, *The Open Civil Engineering Journal*. (2017).  
doi:10.2174/1874149501711011079.
- [12] F. Clementi, V. Gazzani, M. Poiani, S. Lenci, Assessment of seismic behaviour of heritage masonry buildings using numerical modelling, *Journal of Building Engineering*. (2016).  
doi:10.1016/j.jobe.2016.09.005.
- [13] M. Valente, G. Milani, E. Grande, A. Formisano, Historical masonry building aggregates: Advanced numerical insight for an effective seismic assessment on two row housing compounds, *Engineering Structures* (2019), 190, 360-379.
- [14] S. Tiberti, M. Acito, M. Milani, Comprehensive FE numerical insight into Finale Emilia Castle behaviour under 2012 Emilia Romagna seismic sequence: damage causes and seismic vulnerability mitigation hypothesis, *Engineering Structures* (2016), 117, 397-421.
- [15] M. Valente, G. Milani, Damage assessment and collapse investigation of three historical masonry palaces under seismic actions (2019), *Engineering Failure Analysis*, 98, 10-37.
- [16] T.M. Ferreira, R. Maio, R. Vicente, Seismic vulnerability assessment of the old city centre of Horta, Azores: calibration and application of a seismic vulnerability index method, *Bulletin of Earthquake Engineering*. (2017). doi:10.1007/s10518-016-0071-9.
- [17] A. Basaglia, A. Aprile, E. Spacone, F. Pilla, Performance-based Seismic Risk Assessment of Urban Systems, *International Journal of Architectural Heritage*. 12 (2018) 1131–1149.  
doi:10.1080/15583058.2018.1503371.
- [18] G. Grünthal, (Ed.) *Chaiers du Centre Européen de Géodynamique et de Séismologie: Volume 15-European Macroseismic Scale 1998; European Center for Geodynamics and Seismology: Luxembourg, 1998;ISBN 2879770084*
- [19] D. Rapone, G. Brando, E. Spacone, G. De Matteis, Seismic vulnerability assessment of historic centers: description of a predictive method and application to the case study of scanno (Abruzzi, Italy), *International Journal of Architectural Heritage*. 12 (2018) 1171–1195.  
doi:10.1080/15583058.2018.1503373.
- [20] Savini Patrizio, *Storia della città di Camerino*, Second, Tipografia Sarli, 1864.
- [21] L. Chiaraluce, R. Di Stefano, E. Tinti, L. Scognamiglio, M. Michele, E. Casarotti, M. Cattaneo, P. De Gori, C. Chiarabba, G. Monachesi, A. Lombardi, L. Valoroso, D. Latorre, S. Marzorati, The 2016 Central Italy Seismic Sequence: A First Look at the Mainshocks, Aftershocks, and Source Models, *Seismological Research Letters*. (2017). doi:10.1785/0220160221.

- 1535  
1536  
1537  
1538  
1539  
1540  
1541  
1542  
1543  
1544  
1545  
1546  
1547  
1548  
1549  
1550  
1551  
1552  
1553  
1554  
1555  
1556  
1557  
1558  
1559  
1560  
1561  
1562  
1563  
1564  
1565  
1566  
1567  
1568  
1569  
1570  
1571  
1572  
1573  
1574  
1575  
1576  
1577  
1578  
1579  
1580  
1581  
1582  
1583  
1584  
1585  
1586  
1587  
1588  
1589  
1590  
1591  
1592  
1593
- [22] INGV, Rapporto Di Sintesi Sul Terremoto in Centro Italia Mw 6.5 del 30 Ottobre 2016, Gruppo Di Lavoro INGV Sul Terremoto in Centro Italia. (2016) 1–49. doi:10.5281/zenodo.166019.
- [23] National Institute of Geophysics and Vulcanology, Prime interpretazioni dall’interferogramma differenziale ottenuto da dati radat del satellite europeo Sentinel-1, 2016. <https://ingvterremoti.wordpress.com>.
- [24] P. Mouroux, B. Le Brun, Presentation of RISK-UE project, Bulletin of Earthquake Engineering. (2006). doi:10.1007/s10518-006-9020-3.
- [25] A. Formisano, G. Florio, R. Landolfo, F.M. Mazzolani, Numerical calibration of an easy method for seismic behaviour assessment on large scale of masonry building aggregates, Advances in Engineering Software. (2015). doi:10.1016/j.advengsoft.2014.09.013.
- [26] N. Chieffo, A. Formisano, Geo-Hazard-Based Approach for the Estimation of Seismic Vulnerability and Damage Scenarios of the Old City of Senerchia (Avellino, Italy), Geosciences. 9 (2019) 59. doi:10.3390/geosciences9020059.
- [27] N. Chieffo, A. Formisano, The Influence of Geo-Hazard Effects on the Physical Vulnerability Assessment of the Built Heritage: An Application in a District of Naples, Buildings. 9 (2019) 26. doi:10.3390/buildings9010026.
- [28] D. Benedetti, V. Petrini, Sulla vulnerabilità si sismica di edifici in muratura: Un metodo di valutazione, L’Industria Delle Costruzioni. (1984).
- [29] N. Chieffo, A. Formisano, T. Miguel Ferreira, Damage scenario-based approach and retrofitting strategies for seismic risk mitigation: an application to the historical Centre of Sant’ Antimo (Italy), European Journal of Environmental and Civil Engineering. 0 (2019) 1–20. doi:10.1080/19648189.2019.1596164.
- [30] S. Lagomarsino, S. Giovinazzi, Macroseismic and mechanical models for the vulnerability and damage assessment of current buildings, Bulletin of Earthquake Engineering. 4 (2006) 415–443. doi:10.1007/s10518-006-9024-z.
- [31] T.M. Ferreira, R. Vicente, H. Varum, Seismic vulnerability assessment of masonry facade walls: Development, application and validation of a new scoring method, Structural Engineering and Mechanics. (2014). doi:10.12989/sem.2014.50.4.541.
- [32] R. Vicente, T. Ferreira, R. Maio, Seismic Risk at the Urban Scale: Assessment, Mapping and Planning, Procedia Economics and Finance. 18 (2014) 71–80. doi:10.1016/S2212-5671(14)00915-0.

- 1594  
1595  
1596  
1597  
1598  
1599  
1600  
1601  
1602  
1603  
1604  
1605  
1606  
1607  
1608  
1609  
1610  
1611  
1612  
1613  
1614  
1615  
1616  
1617  
1618  
1619  
1620  
1621  
1622  
1623  
1624  
1625  
1626  
1627  
1628  
1629  
1630  
1631  
1632  
1633  
1634  
1635  
1636  
1637  
1638  
1639  
1640  
1641  
1642  
1643  
1644  
1645  
1646  
1647  
1648  
1649  
1650  
1651  
1652
- [33] T. Crespellani, C.A. Garzonio, Seismic risk assessment for the preservation of historical buildings in the city of Gubbio, in: *Geotechnical Engineering for the Preservation of Monuments and Historic Sites: Proceedings of the International Symposium on Geotechnical Engineering for the Preservation of Monuments and Historic Sites, Napoli, Italy, 3-4 October 1996, 1997.*
- [34] E. Guagenti, V. Petrini, The Case of Old Buildings: Towards a New Law - Intensity Damage, in: *Proceedings of the 12th Italian Conference on Earthquake Engineering—ANIDIS. Italian National Association of Earthquake Engineering, Pisa, Italy (in Italian)., 1989.*  
doi:10.1017/CBO9781107415324.004.
- [35] DM 17/01/2018, Aggiornamento delle “Norme Tecniche per le Costruzioni” - NTC 2018, (2018) 1–198.
- [36] S.T.A data srl, 3Muri 10.9.0 - User Manual, (n.d.).
- [37] Q. Piattoni, E. Quagliarini, S. Lenci, Experimental analysis and modelling of the mechanical behaviour of earthen bricks, *Construction and Building Materials.* (2011).  
doi:10.1016/j.conbuildmat.2010.11.039.
- [38] A. Formisano, Theoretical and Numerical Seismic Analysis of Masonry Building Aggregates: Case Studies in San Pio Delle Camere (L’Aquila, Italy), *Journal of Earthquake Engineering.* (2017).  
doi:10.1080/13632469.2016.1172376.
- [39] A. Formisano, Local- and global-scale seismic analyses of historical masonry compounds in San Pio delle Camere (L’Aquila, Italy), *Natural Hazards.* (2017). doi:10.1007/s11069-016-2694-1.
- [40] F. Clementi, A. Pierdicca, A. Formisano, F. Catinari, S. Lenci, Numerical model upgrading of a historical masonry building damaged during the 2016 Italian earthquakes: the case study of the Podestà palace in Montelupone (Italy), *Journal of Civil Structural Health Monitoring.* 7 (2017) 703–717. doi:10.1007/s13349-017-0253-4.
- [41] Eurocode 8, European Standard EN 1998-3:2005: Design of structures for earthquake resistance - Part 3: Assessment and retrofitting of buildings, Comite Europeen de Normalisation, Brussels. (2005).
- [42] Z. V. Milutinovic, G.S. Trendafiloski, WP4: Vulnerability of current buildings. Risk-UE project Handbook, European Commission. (2003). doi:10.1007/978-1-4020-3608-8\_23.